Results in Physics 12 (2019) 2136–2140

Contents lists available at ScienceDirect

Results in Physics

journal homepage: www.elsevier.com/locate/rinp

Area-selective electrodeposition of micro islands for $CuInSe_2$-based photovoltaics

David Correia[a,1], Daniel Siopa[b,1], Diego Colombara[a], Sara Tombolato[b], Pedro M.P. Salomé[a], Kamal Abderrafi[a], Pedro Anacleto[a], Phillip J. Dale[b], Sascha Sadewasser[a,*]

[a] International Iberian Nanotechnology Laboratory (INL), 4715-330 Braga, Portugal
[b] Physics and Materials Science Research Unit, University of Luxembourg, L-4422 Belvaux, Luxembourg

ARTICLE INFO

Keywords:
Electrodeposition
Ultra-micro electrodes
$Cu(In,Ga)Se_2$
Solar cells

ABSTRACT

For mass fabrication of highly-efficient photovoltaic modules based on $Cu(In,Ga)Se_2$ (CIGSe) absorber layers the availability and cost of the critical raw materials In and Ga present a potential bottleneck. The micro-concentrator solar cell concept provides a solution by using micro lenses to concentrate incoming sun light on an array of micro-sized CIGSe solar cells. The challenge is to fabricate CIGSe micro islands in exactly the desired positions using only the required material. Here, we analyze the area-selective electrodeposition of $CuInSe_2$ into holes in an insulating SiO_2 template layer as a material-efficient fabrication approach. We observe that the deposition process shows a strong dependence on the hole size, with a faster deposition around the hole perimeter. Based on a model developed for electrochemical reactions at ultra-micro electrodes, we develop numerical simulations for the electrochemical deposition process. The simulations consider the changing micro-electrode geometry throughout the deposition process, and provide a reasonable fit to the experimental data. Finally, it is shown that $CuInSe_2$ micro solar cells fabricated by electrodeposition reach efficiencies of 4.8% under 1 sun, providing a proof-of-concept demonstration meriting further development.

Introduction

$Cu(In,Ga)Se_2$ (CIGSe) solar cells reach the highest power conversion efficiency of all thin-film photovoltaic technologies, with the present record at 22.9% [1,2]. The CIGSe absorber layer in highly efficient cells is deposited under vacuum, either by co-evaporation from elemental precursors [3] or by sputtering and subsequent reaction in selenium and/or sulfur atmosphere [2]. However, the availability and cost of In and Ga have been raised as a concern for large-scale fabrication and installation of CIGSe PV [4]. The micro-concentrator solar cell concept [5,6] has been proposed as a way to reduce the amount of In and Ga in CIGSe devices. The strategy is to use ordered micro lenses to concentrate the impinging sunlight on a regular array of micrometer-sized CIGSe solar cells. For example, considering a perfect collection of all the impinging sunlight concentrated by a factor of 100 onto micro solar cells, this concept promises to reduce the amount of the critical raw materials In and Ga by the same factor, which is a considerable materials savings. Proof-of-concept devices have been prepared by lithographically defining micro cells from evaporated CIGSe material and have shown efficiencies of up to 21.3% under 475x [6]. More recently, proof-of-concept line-shaped [7] and micro-island [8] CIGSe devices have demonstrated the full materials-saving potential of the concept, leading to efficiencies of ~5% and ~0.3%, respectively. In both cases, the micrometer-sized absorbers were realized by selective area electrodeposition on confined Mo electrodes.

For large area electrodes, the current (I_C) of an electrochemical process in solution depends essentially on the bulk concentration of the species j involved (C_j^0), its diffusion coefficient (D_j), and the number of electrons (n) transferred in the process, as described by Cottrell [9]:

$$I_C = \frac{n\ F\ A\ C_j^0 \sqrt{D_j}}{\sqrt{\pi t}} \quad (1)$$

where t is the deposition time, F the Faraday constant, and A the area of deposition. The Cottrell equation applies for the deposition after a voltage change between the electrodes and for situations where the supply of the depositing species is limited by their diffusion in solution.

When using a rotating disk electrode (RDE), the supply of species can be faster and the deposition follows the Levich equation [10]:

$$I_L = 0.62\ n\ F\ A\ D^{2/3}\ \omega^{1/2}\ \nu^{-1/6}\ C \quad (2)$$

* Corresponding author.
E-mail address: Sascha.Sadewasser@inl.int (S. Sadewasser).
[1] These authors contributed equally to this work.

https://doi.org/10.1016/j.rinp.2019.02.047
Received 14 February 2019; Accepted 15 February 2019
Available online 20 February 2019

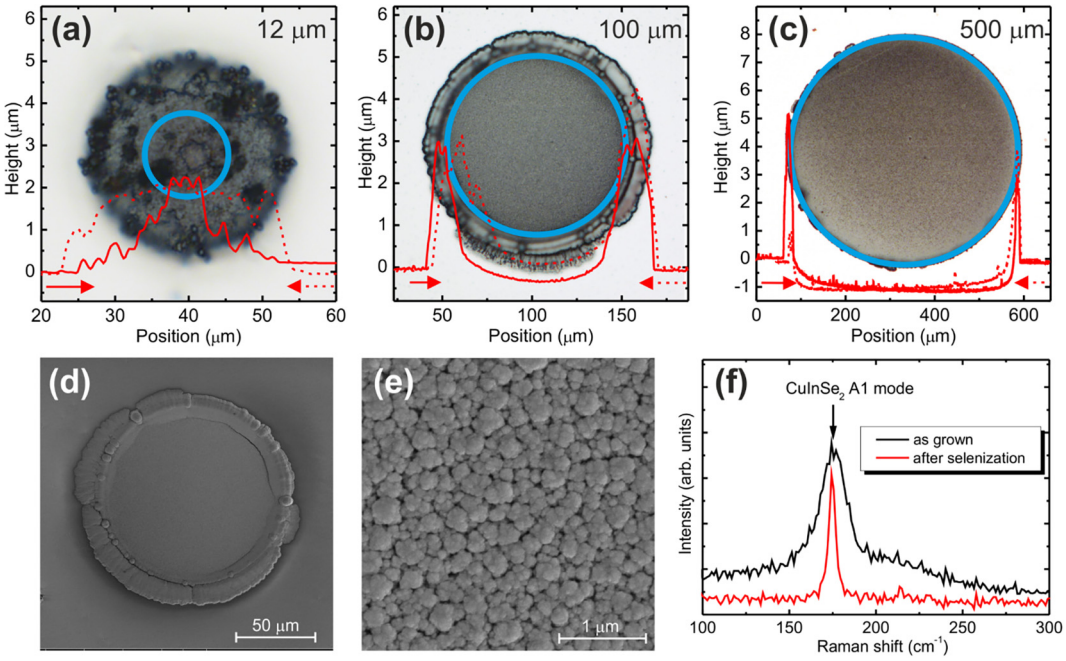

Fig. 1. Electrodeposition of $CuInSe_2$ into holes of (a) 12 μm, (b) 100 μm, and (c) 500 μm diameter in a SiO_2 matrix. For each diameter, an optical microscopy image is shown as the background and profilometer measurements show the thickness of the deposited $CuInSe_2$ for two scan lines (forward – solid line, backward - dashed line). The blue circle indicates the original hole in the SiO_2 matrix. (d) Overview SEM image of a 100 μm hole with the $CuInSe_2$ deposit and (e) high-magnification image of the typical morphology of electrodeposited $CuInSe_2$. (f) Micro-Raman spectroscopy of the $CuInSe_2$ deposited inside a hole, clearly showing the typical A1 vibrational mode.

where ω is the angular rotation rate of the electrode and ν is the kinematic viscosity.

However, local electrochemical processes require special consideration of the geometry for their correct description, such as the case here, electrodepositing into arrays of micro-disk shaped electrodes. For the case of spatially confined electrochemical reactions, in the 1980s Wightman [11] and Fleischmann [12] introduced the concept of ultramicro electrodes (UME), which are generally considered to be ~20 μm or smaller. In this case, the species can only react in specific, locally confined areas and diffusion occurs also laterally, from areas where no reaction can occur to those where the reaction takes place. The overall reaction rate then depends on the number N of disk-shaped UMEs, for which the total electrochemical current is [13,14]:

$$I_{UME} = i\ N = 4\ r\ n\ F\ D\ C\ N \tag{3}$$

where r is the radius of the micro electrodes. Eq. (3) applies for a flat electrode design. For the case of recessed UMEs, a correction factor considering the depth of the electrode has to be included and the current becomes:

$$I_{UME-r} = i\ N = 4\ r\ n\ F\ D\ C\ N\left(\frac{\pi\ r}{4\ L + \pi\ r}\right) \tag{4}$$

where L is the depth of the electrode.

In this work, we investigate the deposition of $CuInSe_2$ [15] into holes created in a SiO_2 insulating coating on top of a conductive substrate. We show that the deposition depends strongly on the hole size. Therefore, we extend the equation describing electrochemical reactions at UMEs to the case of electrodeposition. Finally, we show completed proof-of-concept CIGSe micro solar cell devices obtained by electrodeposition in 200 μm-sized holes in SiO_2.

Experimental

To realize an area-selective electrodeposition process, we fabricated a patterned substrate allowing exposure to the deposition solution only in desired locations of the electrode surface. These pre-structured substrates consist of a soda lime glass sheet (1 mm thickness) with a Mo metallic contact (500 nm thickness deposited by sputtering). A 2 μm thick SiO_2 layer is deposited by plasma-enhanced chemical vapor deposition. Photolithography using a direct write laser is used to pattern a resist, followed by a reactive ion etching to etch the SiO_2 layer down to the Mo contact. The remaining resist is removed using plasma ashing, followed by rinsing with acetone. Details about the fabrication process can be found in Ref. [8]. For the present study, we fabricated a series of holes with diameters ranging from 4 μm to 500 μm.

The electrodeposition of $CuInSe_2$ is realized potentiostatically using a three-electrode cell setup with a saturated calomel reference electrode (SCE). The counter electrode is a 3 × 3 cm^2 Pt mesh and the working electrode is the pre-structured substrate with the series of holes. For all depositions a potential of −0.55 V vs. SCE was applied and the solution was stirred at 60 rpm. The sulfate-based solution contained 2 mM $CuSO_4$, 3.89 mM $In_2(SO_4)_3$, 4.0 mM SeO_2, and 0.26 M Li_2SO_4 as supporting electrolyte [16]. The $CuInSe_2$ micro islands were subsequently selenized for 15 min at 500 °C in a tube furnace; a Se atmosphere was ensured by providing elemental Se as a precursor powder.

For the preparation of micro solar cell devices, the sequential electrodeposition process was chosen to allow the additional incorporation of Ga in the future. To avoid any influence of differently-sized holes, substrates with arrays of identical holes were prepared according to the above described procedure. Initially, Cu was deposited into the holes using a rotating disk electrode (RDE) and a basic Cu solution containing 3.0 M NaOH, 0.2 mM sorbitol, and 0.1 M $CuSO_4$. A deposition voltage of −1.15 V vs. a Ag/AgCl reference electrode was used. Subsequently, In and Ga were deposited simultaneously in an In-Ga electrolyte with 50 mM $InCl_3$ and 25 mM $GaCl_3$ in reline mixture of choline chloride and urea. The deposition was performed at 60 °C inside a N_2-filled glovebox. Details about the electrodeposition can be found in Ref. [17]. To convert the Cu-In-Ga metallic precursor stack into CIGSe, the samples were pre-annealed for 30 min at 100 °C, followed by a selenization step of 20 min at 450 °C using an elemental Se source. To ensure good electrical performance, a KCN etch was performed to remove any residual $Cu_{2-x}Se$ phases. Complete solar cell devices were

then fabricated by a standard CdS chemical bath deposition (50–70 nm thickness) and sputtering of a 90 nm thick i-ZnO and a 350 nm thick ZnO:Al layer [18].

Results

Deposition of $CuInSe_2$ micro islands

The simultaneous deposition of Cu, In, and Se was realized on substrates containing a series of micro electrodes with diameters ranging from 4 μm to 500 μm. The micro electrodes consist of a Mo electrode at the bottom of a hole in a SiO_2 insulating layer of 2 μm thickness. Fig. 1(a)–(c) show exemplary results of the electrodeposition process for holes with diameter of 12 μm, 100 μm, and 500 μm, respectively. The optical microscopy images show clearly that the deposition only occurs at the position of the electrodes and not on the SiO_2 matrix, according to expectation. This was independently confirmed by scanning electron microscopy (SEM) imaging (Fig. 1(d)). The typical microstructure of the $CuInSe_2$ electrodeposited material can be observed in the close-up SEM image in Fig. 1(e). Energy dispersive x-ray spectroscopy experiments of the electrodeposited material in the holes confirm the $CuInSe_2$ composition and Raman measurements show clearly the A1 vibrational mode at 172 cm^{-1} of the tetragonal $CuInSe_2$ (Fig. 1(f)) [19]. However, irregular edges of the deposited material are observed, indicating some deposition around the circumference of the holes. The thickness of the deposited $CuInSe_2$ material was measured by profilometry and the respective curves are overlayed on the optical images in Fig. 1(a)–(c). For the smallest sizes, the holes are filled homogeneously and the material has grown out of the hole, see Fig. 1(a). For the larger holes, Fig. 1(b) and (c), we observe a thicker deposit at the perimeter of the holes, while at the center the $CuInSe_2$ material does not reach the thickness of the SiO_2 layer (i.e. 2 μm). The formation of this corona around the perimeter of the holes shows no dependence on the diameter of the hole and an average width of (15.3 ± 5.5) μm is found. The profilometer data is used to extract the thickness of the $CuInSe_2$ layer and the height of the corona; both values are plotted as a function of the hole diameter in Fig. 2(a). While the corona height is independent of the hole size, the thickness of the $CuInSe_2$ deposit at the center of the holes shows a clear decrease for holes with a diameter larger than 60 μm. These results clearly demonstrate the enhanced deposition in smaller holes.

To analyze the obtained results in more detail, we evaluate the Cottrell and Levich equations for the present deposition conditions. The thickness d of the deposited layer can be estimated according to:

$$d = \frac{I\ M\ t}{F\ n\ \rho\ A} \tag{5}$$

where M is the molar mass of the deposited species (336.3 g/mol for $CuInSe_2$), t is the deposition time, ρ the density of the material (5.7 g/cm^3 for $CuInSe_2$), and A the area of deposition. The compound electrodeposition was assumed to be self-limited by the diffusion of the slowest species (Cu, D = $6.5{\cdot}10^{-6}$ cm^2/s). Using the currents I_C and I_L from Eqs. (1) and (2), it is clear that a dependence on the hole size cannot be described by these equations. The two deposition regimes give a constant thickness independent of the area, illustrated by the horizontal dashed lines in Fig. 2(a).

As described above, electrochemical processes at micro electrodes require the use of Eq. (3). The dependence of the deposition thickness for planar (dotted red line) and recessed (depth L = 2 μm, dashed line) micro electrodes on the electrode diameter are also illustrated. While these dependencies apply for electrochemical processes, in the present case it has to be considered that the electrode shape and size change with time as more and more material is being deposited. We therefore performed numerical simulations of the thickness of the deposited material, the results of which are shown by the solid red lines in Fig. 2(a) and (b). Initially, it is considered that the depth L of the recessed electrode decreases with deposition time. The dependence of the correction factor (see Eq. (4)) for recessed electrodes as a function of electrode diameter and recess depth L is illustrated in Fig. 2(c). Once the hole is filled, the material grows on top of the surface, which we approximate by a hemispherical shape where the thickness and the radius of the electrode change. Fig. 2(b) shows the time dependence of the thickness for three different diameters where the numerical simulation for a fixed recess depth of 2 μm (dashed lines) is compared to our simulation for a deposition process with a variable electrode size and shape (solid lines). The thickness of the dot after a 20-minute deposition is extracted from these numerical simulations as a function of the initial electrode diameter, resulting in the solid line of Fig. 2(a).

Our numerical simulation of the deposition process for micro electrodes gives a better qualitative description of the size dependence, compared to the analytical solution for electrochemical processes according to Eqs. (3) and (4) and illustrated schematically in Fig. 3(a) and

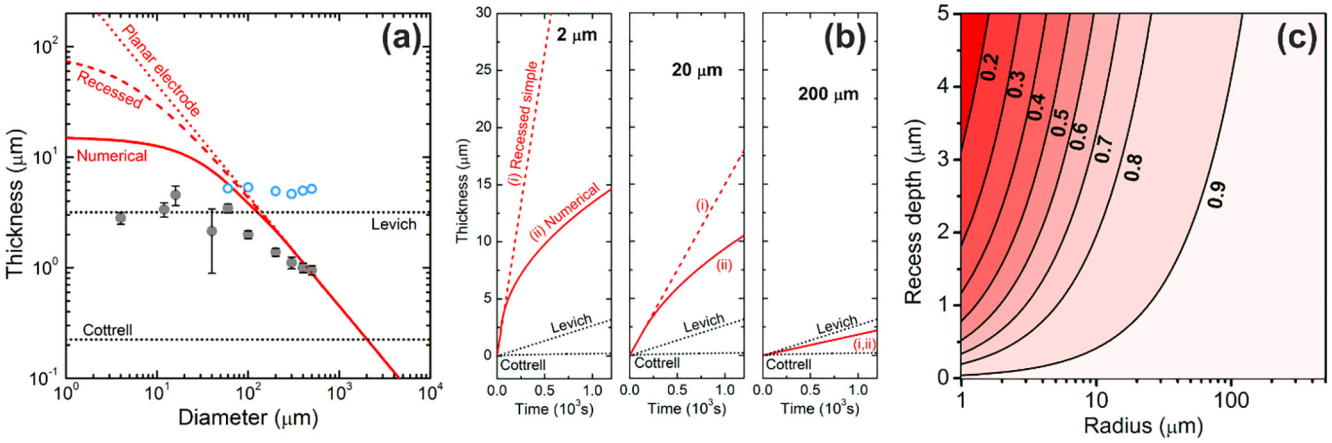

Fig. 2. Electrodeposition in micro-sized holes. (a) Experimental thickness of $CuInSe_2$ at the center of the deposit (solid circles) and the height of the corona (open circles) as a function of microelectrode hole diameter (20 min electrodeposition at 60 rpm). For comparison, the thickness evolution is given for the case of an electrochemical process on a planar electrode (Eq. (3), dotted line), a recessed electrode (Eq. (4), dashed line), and for an actual electrodeposition considering material growth and the changing micro electrode shape and size, according to the numerical simulation shown in (b) (solid line). For comparison, also the Levich (60 rpm) and Cottrell limits are indicated (dotted horizontal lines). (b) Simulated growths of $CuInSe_2$ deposits on micro electrodes of selected sizes, for a fixed recess depth of 2 μm according to Eq. (4) (dashed line) and according to the numerical simulations (solid lines). The growth following the Levich equation for large area electrodes is also given. A 100% plating efficiency is assumed in all cases. (c) Correction factor for recessed micro electrodes as a function of diameter and recess depth according to Eq. (4).

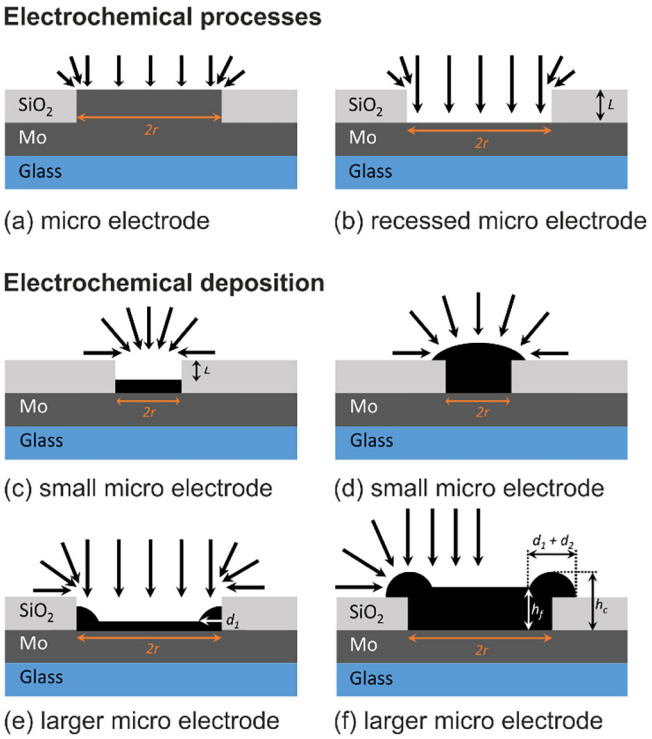

Fig. 3. Schematic illustration of deposition geometry and the diffusion of species in solution for chemical reaction processes above (a) a micro electrode and (b) a recessed micro electrode. For an electrodeposition process, the material being deposited causes changes to the shape and size of the micro electrode during the deposition: (c) A small recessed microelectrode fills up, reducing the recess depth L and eventually (d) the material grows in a hemispherical way out of the micro electrode. For larger micro electrodes, the additional species that arrive from areas where no deposition occurs will lead to a corona effect increasing the thickness of deposited material (e) inside the recessed micro electrode and (f) leading to thicker deposit (h_c) at the circumference of the initially recessed microelectrode.

(b). However, a quantitative agreement is not reached. We attribute the discrepancies to two major reasons. (i) The deposited material in our study is $CuInSe_2$, which is a semiconductor; thus, the growth of the film is accompanied by a voltage drop across the thickness of the electrode, which continuously shifts the effective electrochemical potential to more positive values during plating. (ii) The size range of the electrodes in our study goes beyond the range which is typically considered a micro electrode. In fact, our experimental results for diameters up to 60 µm follow the schematic illustration in Fig. 3(c) and (d), corresponding to what would be expected for a typical micro electrode. Unlike in the Cottrell regime, additional reaction species diffuse from regions outside the electrode, leading to higher currents and – in the case of electrodeposition – thicker deposited material. If the diameter of the electrode becomes larger, the diffusion of these species does not cover the full electrode anymore and enhanced deposition only occurs at the outer ring of the electrode. This enhanced deposition leads to the corona effect observed in our study, which is schematically illustrated in Fig. 3(e) and (f). The width of the corona should be related to the diffusion coefficient of the depositing species, independent of the electrode size, in agreement with our experimental observation.

$Cu(In,Ga)Se_2$ micro solar cells

For the fabrication of micro solar cells, we used the sequential deposition of Cu and In, followed by a high–temperature anneal in Se atmosphere to convert the Cu-In precursor into $CuInSe_2$. To test the suitability of the above described electrodeposition process, the deposition of the metallic precursor was performed into the same SiO_2 matrices with holes. An array of 13 × 13 $CuInSe_2$ micro absorbers with a diameter of 200 µm was then processed to full solar cell devices by deposition of CdS and the i-ZnO/ZnO:Al window layers. Subsequently, a single cell was isolated by scratching carefully the window layer stack on top of the SiO_2 matrix around the selected device (Fig. 4(a)). For the measurement of the current density (J)-voltage (V) characteristics, four contacts were placed, two of them on the Mo back contact and the other two directly on the ZnO:Al layer on the SiO_2 insulating layer close to the selected device. The JV characteristics presented in Fig. 4(b) show a well performing solar cell with an open-circuit voltage of V_{oc} = 396 mV, a short-circuit current of J_{sc} = 25.2 mA/cm^2, and a fill factor of FF = 48%, leading to a power conversion efficiency of 4.8%.

These device results clearly show the suitability of the approach to electrodeposit $CuInSe_2$ into holes in an insulating matrix to realize the materials-efficient fabrication of micro-concentrator solar cells. Optimization of the electrodeposition process is required to address the above-described geometry-dependent deposition results.

Conclusion

We have presented a detailed analysis of the electrodeposition process into recessed micro electrodes by extending the analytical equations for electrochemical reactions in microelectrodes using numerical simulations to account for the size and shape change of the electrodes throughout the deposition process. Our results provide a qualitative description of the electrodeposition of $CuInSe_2$ into recessed micro electrodes, which are studied for their application in photovoltaic energy conversion implementing the micro-concentrator thin film solar cell concept. To demonstrate this novel PV concept, $CuInSe_2$ micro solar cells of 200 µm diameter were fabricated and their efficiency was measured to be 4.8% under 1 sun. Our study provides valuable insights into microelectrode electroplating, which is also relevant for many

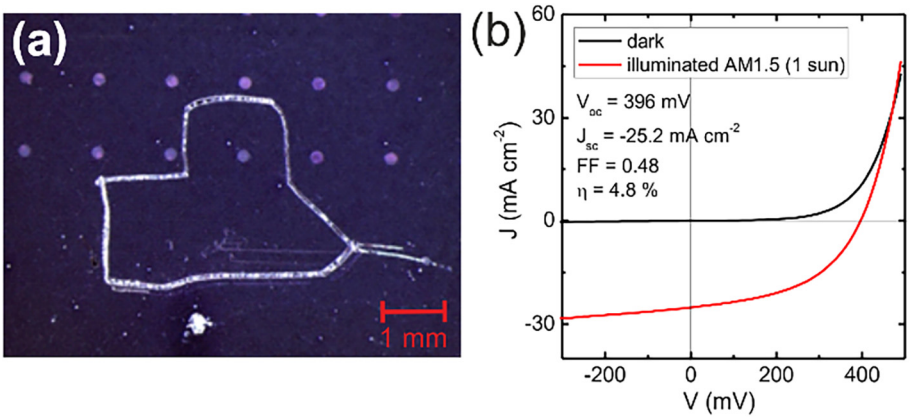

Fig. 4. (a) Optical microscope image of a 6 × 2 subarray of 200 µm-diameter $CuInSe_2$ micro solar cells deposited by a sequential electrodeposition process of Cu and In, followed by selenization. The micro absorbers were processed to devices by deposition of CdS and i-ZnO/ZnO:Al window layers and a single cell was isolated by mechanically scratching the ZnO layers. (b) JV curves in dark and under 1-sun illumination of the isolated 200 µm-diameter solar cell with the extracted solar cell parameters.

other applications from sensing to microfabrication. For the presented micro solar cells, we demonstrated proof-of-concept devices paving the way for further developments of this promising PV concept.

Acknowledgements

This work was partially supported by the project Nanotechnology Based Functional Solutions (NORTE-01-0145-FEDER-000019), supported by Norte Portugal Regional Operational Programme (NORTE2020), under the PORTUGAL 2020 Partnership Agreement, through the European Regional Development Fund (ERDF). We acknowledge additional support by the Micro-concentrator thin film solar cells project (028922), co-funded by FCT and the ERDF through COMPETE2020. Funding by the Luxemburgish Fond National de la Recherche (FNR) through the MASSENA project is gratefully acknowledged. K.A. would like to acknowledge the Marie-Curie-COFUND program NanoTRAINForGrowth (grant agreement N°600375). DC thanks INL and the European Commission for funding the Nano Train for Growth II project n. 713640 through the Marie Curie Cofund programme.

Data availability

The raw/processed data required to reproduce these findings cannot be shared at this time as the data also forms part of an ongoing study.

References

[1] Green MA, Emery K, Hishikawa Y, Warta W, Dunlop ED, Levi DH, et al. Solar cell efficiency tables (version 49). Prog Photovoltaics: Res Appl 2017;25:3–13.
[2] Solar Frontier press release, 20.12.2017, http://www.solar-frontier.com/eng/news/2017/1220_press.html.
[3] Jackson P, Wuerz R, Hariskos D, Lotter E, Witte W, Powalla M. Effects of heavy alkali elements in Cu(In, Ga)Se_2 solar cells with efficiencies up to 22.6%. Phys Status Solidi RRL 2016;10:583–6.
[4] Wadia C, Alivisatos AP, Kammen DM. Environ Sci Technol 2009;43:2072.
[5] Paire M, Lombez L, Donsanti F, Jubault M, Collin S, Pelouard J-L, et al. Thin-film microcells: a new generation of photovoltaic devices. SPIE Newsroom 2013. https://doi.org/10.1117/2.1201305.004808.
[6] Paire M, Lombez L, Donsanti F, Jubault M, Collin S, Pelouard J-L, et al. Cu(In, Ga)Se_2 microcells: high efficiency and low material consumption. J Renew Sustain Energy 2013;5:011202.
[7] Duchatelet A, Nguyen K, Grand P-P, Lincot D, Paire M. Self-aligned growth of thin film Cu(In, Ga)Se_2 solar cells on various micropatterns. Appl Phys Lett 2016;109:253901.
[8] Sadewasser S, Salomé P, Rodriguez-Alvarez H. Materials efficient deposition and heat management of $CuInSe_2$ micro-concentrator solar cells. Sol Energy Mater Sol Cells 2017;159:496–502.
[9] Cottrell FG. Der Reststrom bei galvanischer Polarisation, betrachtet als ein Diffusionsproblem. Z Phys Chem 1903;42U:385–431.
[10] Levich VG. Physicochemical Hydrodynamics. Prentice-Hall; 1962.
[11] Wightman RM. Microvoltammetric electrodes. Anal Chem 1981;53:1125A–34A.
[12] Fleischmann M, Pons S, Rolison DR, Schmidt PP. Ultramicroelectrodes. Morganton, NC: Datatech Systems Inc; 1987.
[13] Bard AJ, Faulkner LR. Electrochemical methods: fundamentals and applications. John Wiley & Sons; 2001.
[14] Stulík K, Amatore Ch, Holub K, Marecek V, Kutner W. Microelectrodes. Definitions, characterization, and applications (Technical report). Pure Appl Chem 2000;72:1483–92.
[15] Chassaing E, Grand P-P, Ramdani O, Vigneron J, Etcheberry A, Lincot D. Electrocrystallization mechanism of Cu–In–Se compounds for solar cell applications. J Electrochem Soc 2010;157(7):D387–95.
[16] Sene C, Calixto ME, Dobson KD, Birkmire RW. Electrodeposition of $CuInSe_2$ absorber layers from pH buffered and non-buffered sulfate-based solutions. Thin Solid Films 2008;516:2188–94.
[17] Malaquias JC, Regesch D, Dale PJ, Steichen M. Simultaneous electrodeposition of indium and gallium from a choline chloride based deep eutectic solvent for Cu(In, Ga)Se_2 solar cells. PCCP 2014;16:2561–7.
[18] Aida Y, Depredurand V, Larsen JK, Arai H, Tanaka D, Kurihara M, et al. $CuInSe_2$ solar cells with a Cu-poor surface. Prog Photovoltaics: Res Appl 2015;23:754–64.
[19] Rincon C, Ramirez FJ. Lattice vibrations of $CuInSe_2$ and $CuGaSe_2$ by Raman microspectrometry. J Appl Phys 1992;72:4321–4.